Available online at www.CivileJournal.org

Civil Engineering Journal

(E-ISSN: 2476-3055; ISSN: 2676-6957)

Vol. 10, No. 09, September, 2024

Frictional Axial Resistance of Clamped Split Pocket Mechanism Steel Structural Joint: An Experimental Study

Whelly T. Putra [1], Angga F. Setiawan [1*], Ashar Saputra [1], Iman Satyarno [1], Hamdi Y. Pratama [1]

[1] *Department of Civil and Environmental Engineering, Universitas Gadjah Mada, Jalan Grafika No. 2, Yogyakarta 55281, Indonesia.*

Received 02 May 2024; Revised 18 August 2024; Accepted 25 August 2024; Published 01 September 2024

Abstract

The Clamped Split Pocket Mechanism (CSPM) prefabricated joint system was developed for a single-story steel instant house, designed to be compact and rapidly constructed without modifying the end of the beam and column element member. The CSPM bolted joint system was proposed as an optimal solution for post-disaster housing, especially after earthquakes. Despite its potential, the frictional tensile resistance behavior of the CSPM bolted joint system has not been previously studied, necessitating experimental investigation. This study examined the frictional tensile resistance behavior of the CSPM joint system by monitoring the effective friction coefficient under axial tension force. The experiments considered both the strong and weak axes of the joint and utilized two configuration types of specimens (L and T) with varying bolt pretensions of 2.5, 5, 7.5, and 10 kN. Results indicated that the effective friction coefficient of the CSPM bolted joint system ranged from 0.19 to 0.26, correlated to bolt pretension. Increased bolt pretension resulted in larger surface deformation of the split pocket, triggering a not uniform frictional tensile resistance across the steel surfaces of the split pocket joint. From this study, the achieved effective friction coefficients could guide the design of minimum pretension forces for clamps in prefabricated steel instant houses.

Keywords: Frictional Axial Resistance; Bolt Pretension; Prefabricated Beam-Column Joint; Steel Instant House; Effective Friction Coefficient.

1. Introduction

Due to high-risk seismic occurrences in developing countries, applying the concept of resilience in non-engineered buildings, especially one-story houses, must be promoted. According to Librian et al. [1], the 2006 Yogyakarta earthquake resulted in 5,700 fatalities, nearly 60,000 injuries, hundreds of thousands of damaged houses, and billions of dollars in losses. Meanwhile, an earthquake in Palu in 2018, followed by a tsunami and liquefaction disaster, resulted in 40,085 lightly damaged houses, 26,122 moderately damaged houses, 30,148 severely damaged houses, and the displacement of 206,494 individuals [2–4]. Most of the heavily damaged or collapsed structures were sustained by one-story houses made of masonry-reinforced concrete. Even though the government has published formal guidelines, ordinary bricklayers cannot easily implement specific reinforcement details. During the post-disaster recovery, repairing damaged or collapsed houses demands high effort, labor, time, and finances [5, 6]. Therefore, applying a new concept incorporating light and ductile structural designs for one-story houses is highly needed, along with techniques to achieve the rapid and effective method of reconstructing collapsed houses after the occurrence of earthquakes.

* Corresponding author: angga.fajar.s@ugm.ac.id

http://dx.doi.org/10.28991/CEJ-2024-010-09-07

One alternative is implementing a single-story steel instant house [7]. The instant steel house (RISBA) employs the "*build back better*" concept to enable victims of natural disasters to promptly leave evacuation centers, return home, and rebuild better. The steel instant house utilizes double-channel steel sections of CNP 95 × 33 × 10 × 1.8 with welding construction methods at each joint system. Installing the steel instant house requires five days with five workers per day [7]. To achieve construction that is easy, fast, effective, efficient, and of high quality, the development of the RISBA prefabricated house system is necessary. A qualified mechanical joint system needs to be developed to realize the prefabricated house structure.

Prefabricated joint systems for building structures have been developed, including a prefabricated system using H beams and IWF cross-sections [8, 9]. One example of a developed prefabricated system uses a sleeve with a welding system [7]. However, this has a disadvantage in that experts are required to weld the joints in the field. Apart from the system above, prefabricated systems with bolted joints have also been developed. The bolted joint system demonstrates higher fatigue and tensile strength than welded joints [10]. Prefabricated systems with bolted joints have advantages, such as a more rapid installation, ease of assembly and disassembly, low cost, and do not require skilled labor during installation [8, 11–14]. However, such a system for one-story house structures has yet to be fully developed. Therefore, the development of prefabricated joint systems for such structures must be realized.

Meanwhile, another example of a prefabricated system with a pocket mechanism was developed with a pipe model or circular profile [15]. However, just like the others, this pipe system has disadvantages, such as heavy cross-section, which makes installation by human labor difficult; high cost; and the complex process of assembling structural joints and architectural components. Prefabricated bolted joint systems are strength-dependent on the frictional tensile resistance for axial tensile, in which the torsional moment and the friction coefficient control the frictional tensile resistance.

However, the slip that occurs is one challenge in applying the frictional tensile resistance mechanism to a bolted joint system [16]. One of the causes of slide-in bolt joints is a sufficiently large bolt hole and a high number of bolt joints, often resulting in considerable lateral displacement. This lateral displacement might damage the beam-column joints through the P-delta effect [16]. The mechanism of frictional resistance can be observed through the behavior of the force-displacement (F–d) relationship. As such, the behavior of shear-slip loads through F-d must be studied accurately. To limit cumulative slip displacement to a minimum, the initial F-d behavior for the development of joints for prefabricated steel buildings must include assembly tolerances in the field. In particular, the most crucial parameter for calculating the number of bolts in a bolted joint is the friction coefficient and the treatment of the joint pocket surface [17]. The slip factor approximates the friction coefficient, which is experimentally determined by testing standard specimens. Typically, the behavior of F-d is assumed to be linear, with an arbitrary initial stiffness that varies depending on the slip load and assumed slip displacement.

Limited research has been conducted on the frictional tensile resistance of the CSPM bolted joint system. Still, there have been numerous studies on the frictional tensile resistance of bolted joint systems. For example, Cruz et al. investigated the slip factor of slip-resistant bolted joints with different types of steel (high-strength, low-strength, and weathering steel) and the impact of various surface treatments. The results showed that different steel grades and surface treatments lead to different friction coefficients [18]. Lacey et al. conducted experimental and numerical studies on the slip factor for G350 steel bolted joints and found that different surface treatment layers result in different slip factors [19]. Heistermann et al. examined the effect of slip factors on slip-resistant bolted joints with long slotted holes, considering the impact of different surface treatments on S275 and S690 steel grades. The study indicated that different surface treatments and weather conditions significantly affect the slip factors, while the steel grade has a minor impact [20]. Wang et al. discovered that surface treatment and roughness influence the slip factor of hybrid joints between shot-blasted mild steel and high-strength steel surfaces [21]. Investigating the axial frictional resistance of bolted joints in various structures is crucial to prevent steel member separation from the bolted joint, which can lead to local failure and ultimately cause the entire building structure to fail [22]. Collini et al. conducted an experimental study on the relationship between bolt torque and the effect of surface treatment on the friction coefficient in pretension bolted joints. The results showed that increasing bolt tightening torque reduces the friction coefficient by 10-15%. The friction coefficient for COR-TEN-treated steel surfaces was higher (0.372 ± 0.031) compared to Zn-coated steel (0.298 ± 0.030) and rolled steel (0.242 ± 0.026) [23].

The existing research above has mainly focused on the frictional tensile resistance in ordinary bolted joints, specifically using a slip-resistant bolted joints model between two steel plates in contact. The existing approach has provided frictional tensile resistance values for fixed bolt systems. However, frictional tensile resistance between two sliding steel surfaces must still be addressed. Previous studies have examined different grades of steel and the impact of various surface treatments [18–21, 23]. However, they have mainly focused on experimental testing and numerical modeling of frictional tensile resistance on two steel surfaces experiencing uniformly distributed forces. The frictional tensile resistance values obtained from previous studies cannot be fully applied to the design of bolted joint systems using the CSPM joint model. The reason is that previous research on slip-resistant bolted joints has not yet examined

the frictional tensile resistance, which is not uniformly distributed across two steel surfaces. Additionally, the impact of deformation on the CSPM joint system due to bolt pretension has yet to be considered in earlier studies. Therefore, a study of the frictional tensile resistance of the CSPM bolt joint system needs to be carried out.

This study investigates the frictional tensile resistance behavior of a CSPM used as a beam-column joint system in a prefabricated steel instant house. The effective friction coefficient of CSPM is the main parameter that needs to be investigated. It is important to control the bolt pretension to accommodate appropriate tensile axial forces and prevent damage to the pocket joint surface due to the over-torque of the bolt [24]. The experiments considered both the strong and weak axes of the joint and utilized two types of test specimens (L and T) with varying bolt pretensions (2.5, 5, 7.5 and 10 kN). The outcomes will include F-d curves, friction coefficient values, and the influence of surface conditions on frictional tensile resistance. The analysis of frictional tensile resistance tests will determine the effect of bolt pretension on the slip factor for the joints in prefabricated steel instant houses. This study expected to estimate the appropriate clamping force to achieve axial resistance in such structures' CSPM bolted joint systems.

2. CSPM as a Beam-Column Bolted Joint System

Instant housing systems using prefabricated steel and CSPM beam-column bolted joint systems offer an alternative to modular steel structures (see Figure 1). The CSPM bolted joint system includes columns, beams, split pockets, whole pockets, clamps, stiffeners, and high-strength bolts (refer to Figure 2). The column and beam components are of a lipped channel cross-section type (CNP) spot-welded on the edges, forming a double-lipped channel profile (DCNP) component, and are welded using electric arc welding with RB26-type wire by Kobe Steel. The split pocket is designed with a hollow square (HS) profile split in the middle, while the whole pocket is created from a complete HS profile with notches in the middle axis. Clamps, functioning as fasteners, are installed in both split and whole pockets, with six clamps in each pocket, and are made of plates with holes to accommodate high-quality bolts.

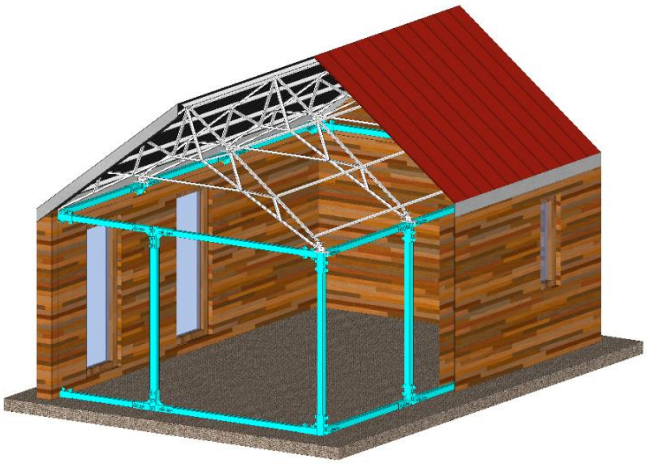

Figure 1. CSPM prefabricated steel instant house

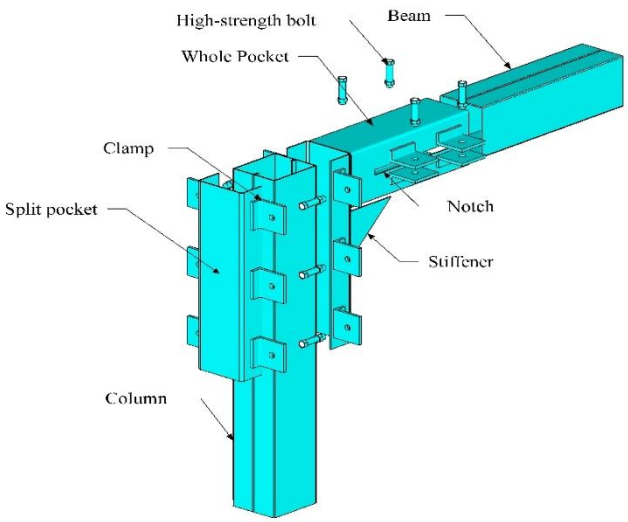

Figure 2. CSPM as a beam-column bolted joint system

3. Research Methods

The research methodology outlined in the flowchart details a systematic approach to investigating the frictional tensile resistance of CSPM bolted joint systems. The flowchart can be seen in Figure 3. The study begins with a comprehensive literature review, which gathers knowledge on bolted joint systems and identifies research gaps, particularly in the context of CSPM bolted joint systems.

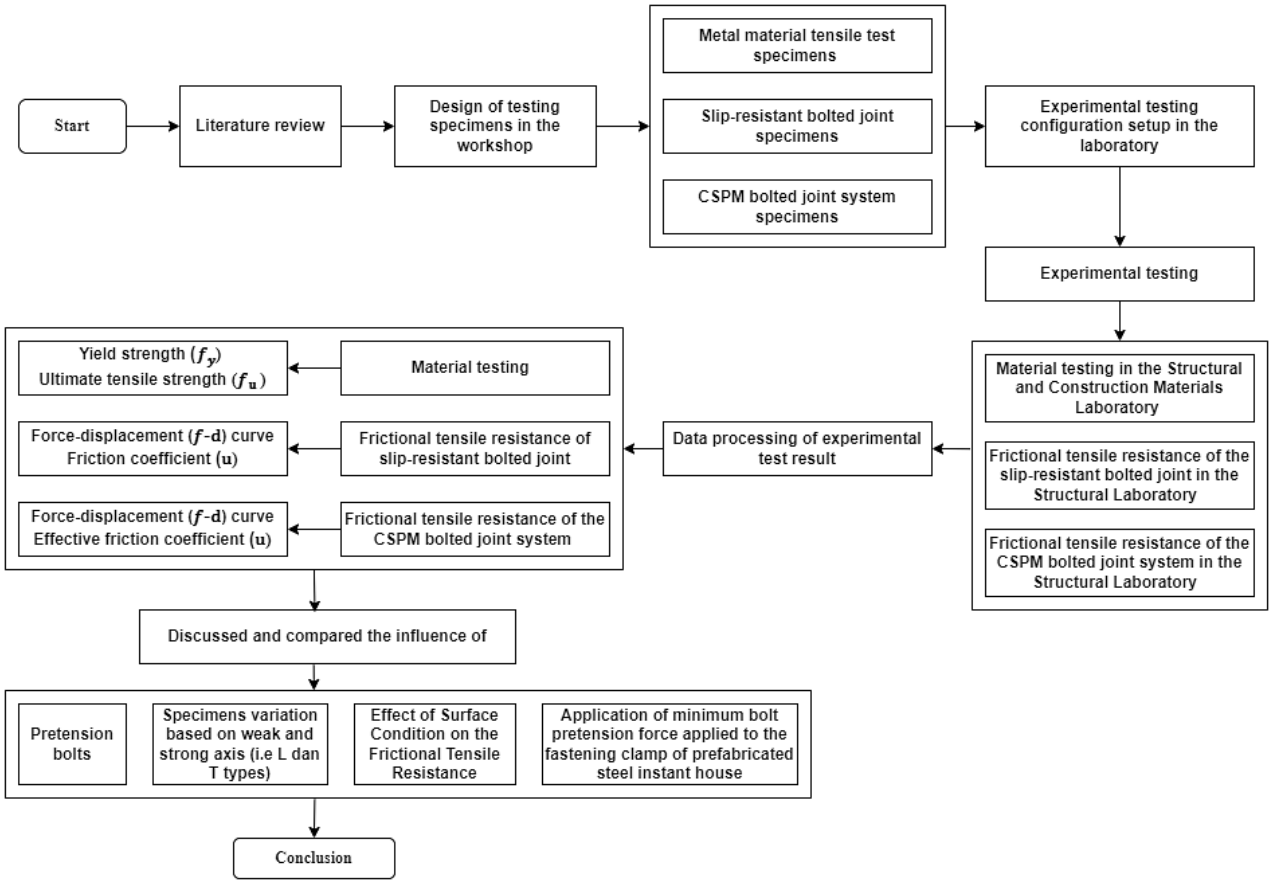

Figure 3. The research flowchart

The workshop conducted the design and fabrication of test specimens. Three types of specimens were prepared: metal material tensile test specimens, slip-resistant bolted joints frictional tensile resistance test specimens, and CSPM bolted joint system frictional tensile resistance test specimens. The metal material tensile test specimens were used to determine the basic properties of the material. The experimental testing phase was tensile material testing of steel, which was performed in the Structural and Construction Materials Laboratory to obtain the yield strength (f_y) and ultimate tensile strength (f_u) of the steel material.

The slip-resistant bolted joints, and CSPM bolted joint system frictional tensile resistance specimens were specifically used to evaluate the friction coefficient under different conditions. Frictional tensile resistance testing of the slip-resistant bolted joints, and CSPM bolted joint system was conducted in the Structural Laboratory. These tests provided data on the force-displacement behavior and friction coefficient, which are essential for understanding the performance of the CSPM bolted joint system under axial tensile loads. Data processing followed the experimental testing, where the results were analyzed to produce force-displacement curves and determine the friction coefficients for the slip-resistant bolted joints and CSPM bolted joint system specimens. The processed data provided insights into the effective friction coefficient (μ) and highlighted performance variations based on different pretension bolt forces and surface conditions.

This study discusses and compares how different factors affect the frictional tensile resistance of the CSPM bolted joint system. These factors include variations in pretension bolts, the orientation of the specimen axis (weak vs. strong axis), and the effect of surface conditions. The findings from this study are expected to determine the variables that impact the performance of the CSPM bolted joint system. The study also recommends applying a minimum bolt pretension force to the clamps of prefabricated steel instant houses to improve their structural integrity and resistance to axial loads.

3.1. Design of Specimens and Parameters for the Friction Axial Tensile Test of the Slip-Resistant Bolted Joints

The frictional tensile resistance test of the slip-resistant bolted joint was conducted on three specimens: HCHTC (hollow square-channel profile-HS without paint and small to large pretension), HCHC-1 (hollow square-channel profile-HS paint and small to large pretension), and HCHC-2 (hollow square-channel profile-HS paint and large to small pretension). The friction tensile resistance of the slip-resistant bolted joint test consisted of three plates: outer plate-1, inner plate, and outer plate-2 (Figure 4). The frictional tensile resistance test specimens for slip-resistant bolted joints follow the methodologies established in previous studies by Cruz et al. [18], Lacey et al. [19], Heistermann et al. [20], Wang et al. [21], and Annan & Chiza [25].

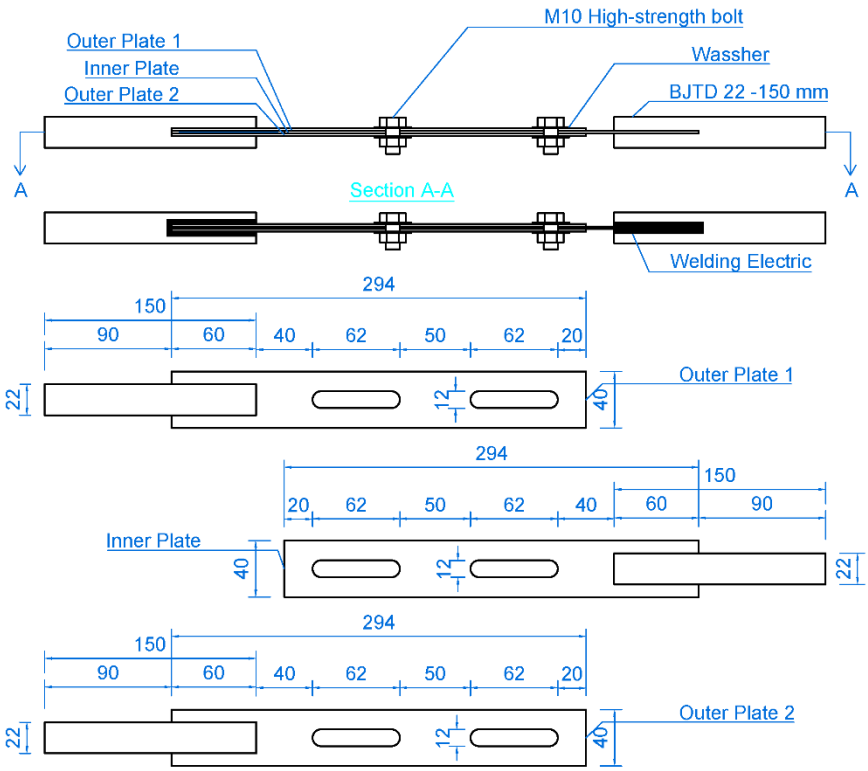

Figure 4. Specimens for frictional tensile resistance testing of slip-resistant bolted joints (all dimensions in mm)

Table 1. Variation in specimens for frictional tensile resistance testing of the slip-resistant bolted joints

Specimens	Outer plate 1	Inner plate	Outer plate 2	Surface treatment	Order of pretension	Pretension (kN)
HCHTC	Hollow square	Channel profile	Hollow square	No painted	Minimum-maximum	1.75
						3.50
						5.25
						7.00
HCHC-1	Hollow square	Channel profile	Hollow square	Zinchromate 2-coat paint	Minimum-maximum	1.75
						3.50
						5.25
						7.00
HCHC-2	Hollow square	Channel profile	Hollow square	Zinchromate 2-coat paint	Maximum-minimum	1.75
						3.50
						5.25
						7.00

The testing parameters for the friction tensile resistance of the slip-resistant bolted joint test are shown in Table 1. The plate used for HS had a thickness of 1.65 mm, while the DCNP plate had a thickness of 1.90 mm. To investigate the repetition of the axial tension load effect, each specimen was multi-tested for axial tension load under four levels of bolt pretension clamping forces. The specimens HCHTC and HCHC-1 were tested with the order of minimum to maximum bolt pretension, while specimen HCHC-2 was tested with the order of maximum to minimum bolt pretension.

3.2. Design of Specimens and Parameters for the Friction Axial Tensile Test of the CSPM Bolted Joint System

The frictional tensile resistance testing of the CSPM beam–column bolted joint system in instant houses made of prefabricated steel was grouped into four different pretension loading scenarios on four different test specimens from the strong–weak axis positions: strong axis T joint (SATJ), weak axis T joint (WATJ), strong axis L joint (SALJ), and weak axis L joint (WALJ). The geometry of the joint system and the details of the CSPM bolted joint systems are shown in Figures 5 and 6, respectively. The test was conducted with a direct load on the strong axis and weak axis of the joint. The parameters of the CSPM bolted joint system friction tensile resistance test specimens are shown in Table 2. The cross-section type used for T and L joints is DCNP with dimensions of 95 × 80 × 10 × 1.8 mm for columns and beams.

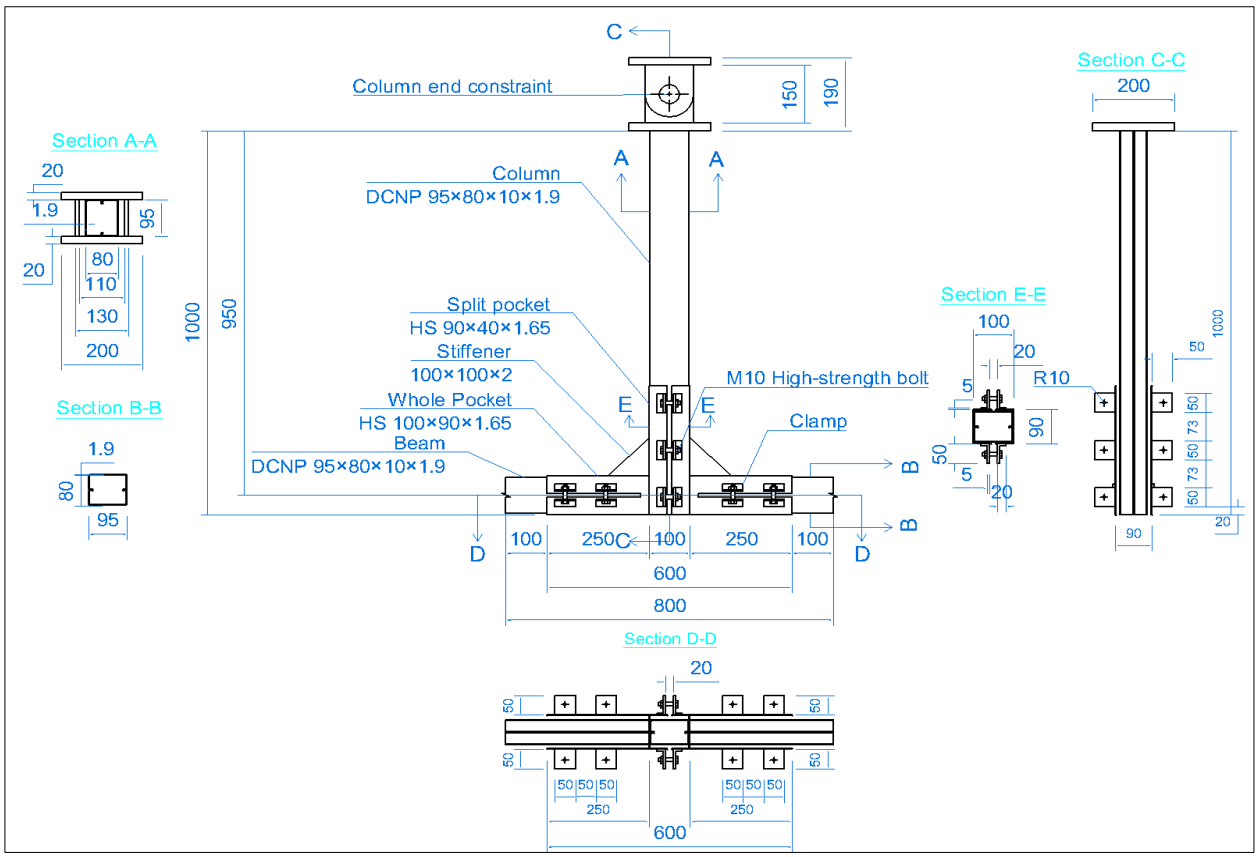

Figure 5. Geometry of the CSPM as a beam-column joint system (all dimensions in mm)

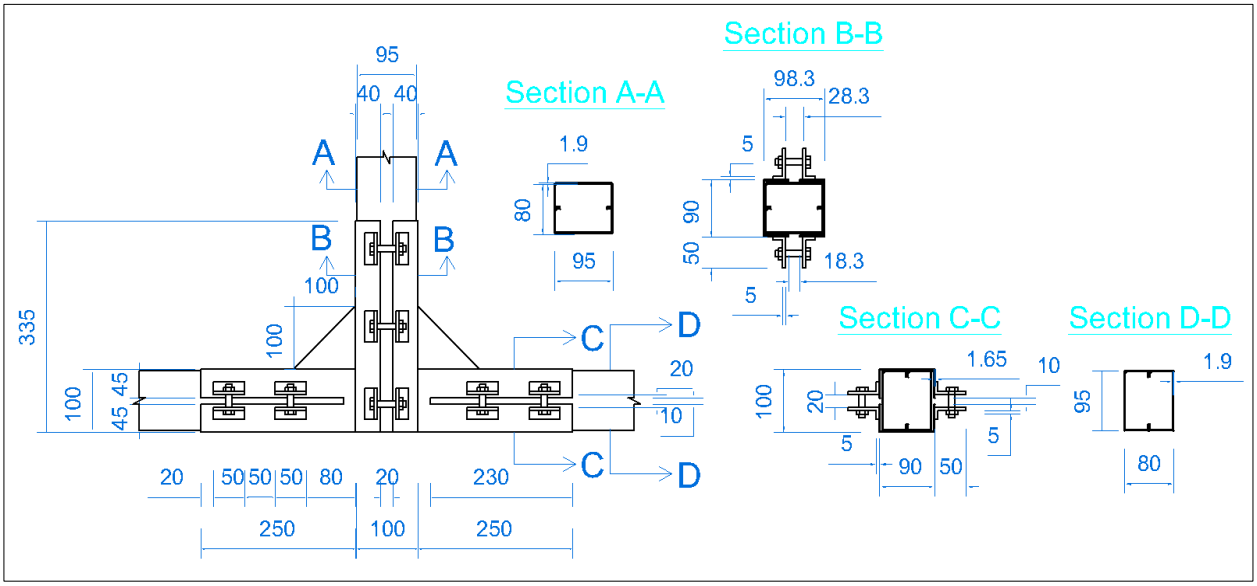

a) Strong Axis T Joints (SATJ) specimen details

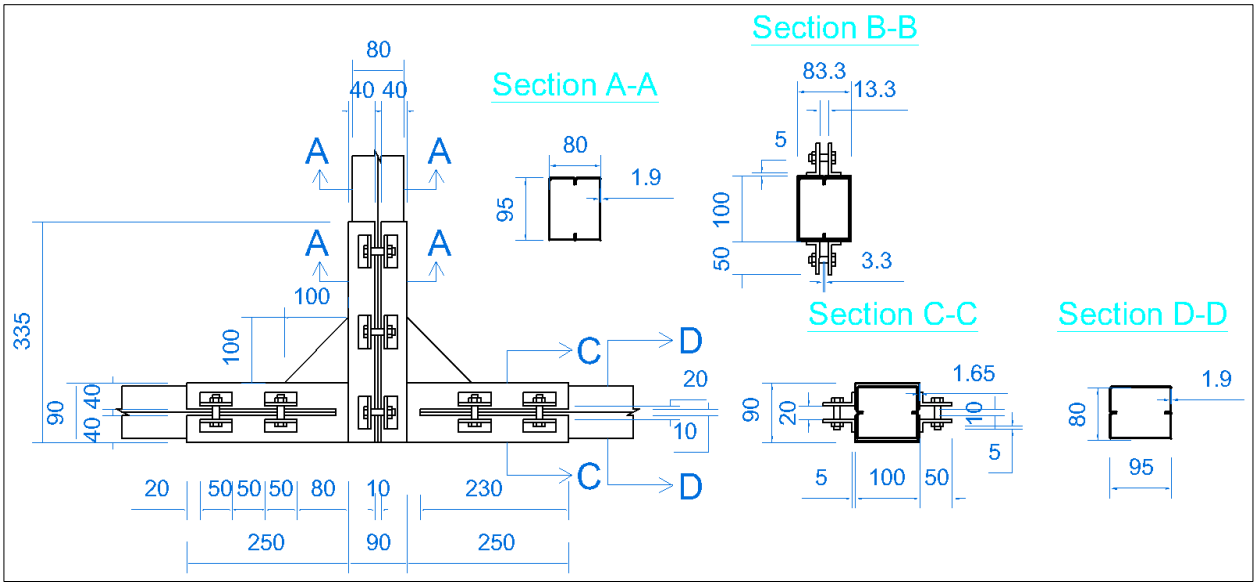

b) Weak Axis T Joints (WATJ) specimen details

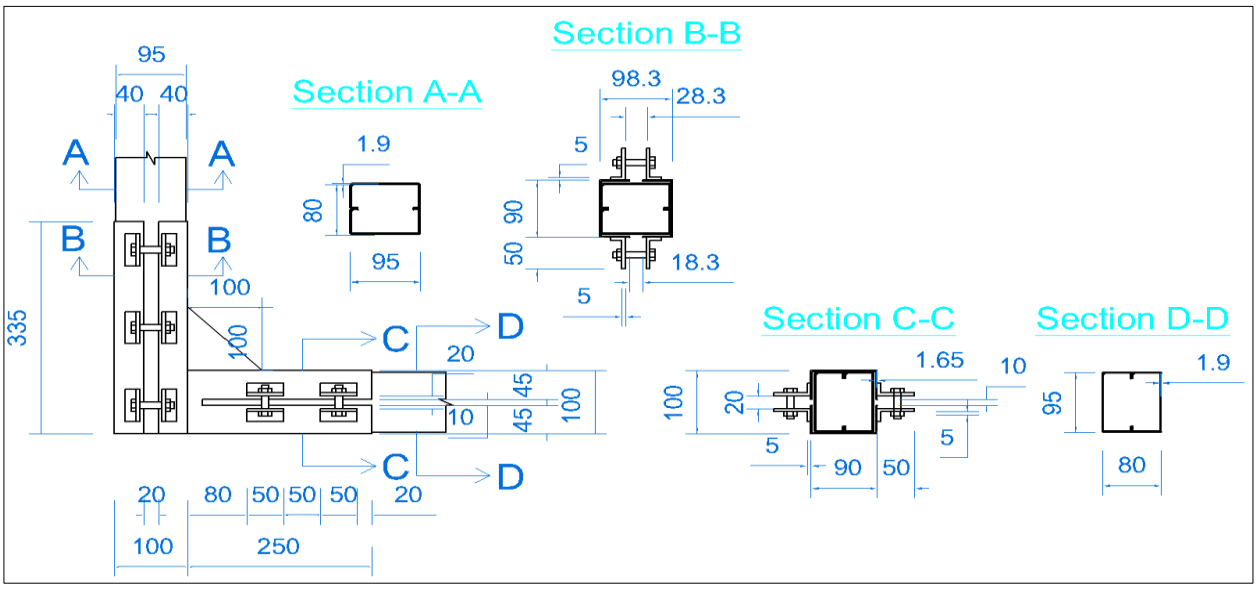

c) Strong Axis L Joints(SALJ) specimen details

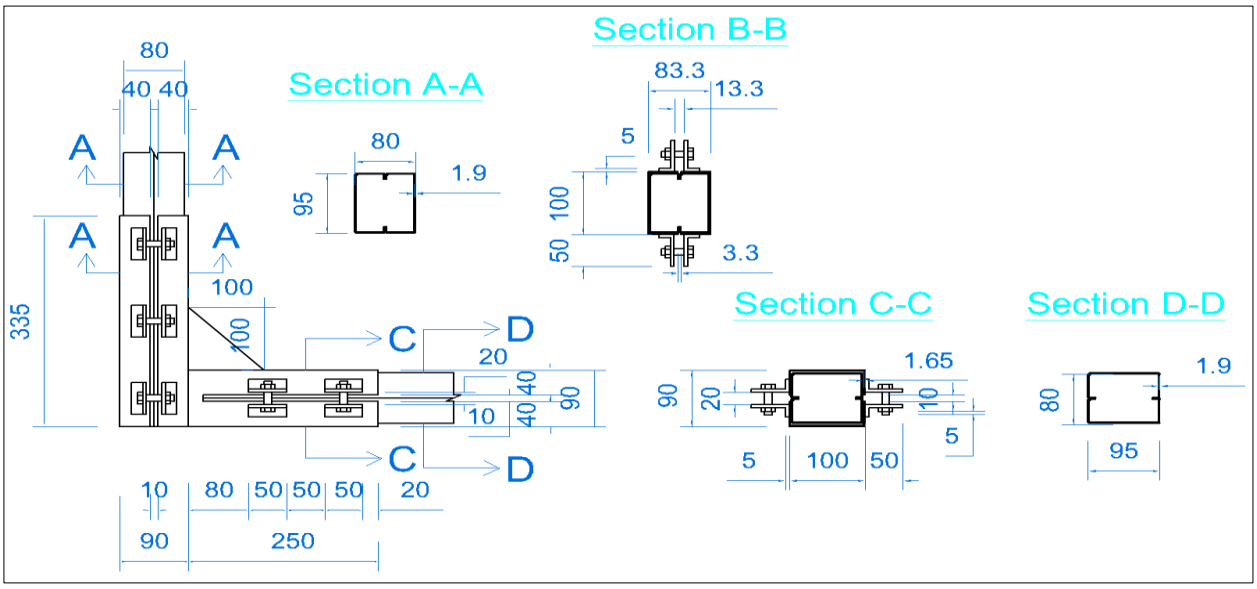

d) Weak Axis L Joints (WALJ) specimen details

Figure 6. Details of CSPM joint system, a) SATJ, b) WATJ, c) SALJ, and d) WALJ (all dimensions in mm)

Table 2. Variation in specimens for the frictional tensile resistance testing of the CSPM bolted joint system

Specimens	Bending axis	Beam and Column (mm)	Stiffener (mm)	Whole pocket		Notch		Split pocket	
				Depth (mm)	Section (mm)	Width (mm)	Depth (mm)	Depth (mm)	Section (mm)
SATJ	Strong	DCNP 95×80×10×1.9	100×100×2	250	HS 100×90 1.65	10	230	335	HS 90×40×1.65
WATJ	Weak	DCNP 95×80×10×1.9	100×100×2	250	HS 100×90 ×1.65	10	230	335	HS 90×40×1.65
SALJ	Strong	DCNP 95×80×10×1.9	100×100×2	250	HS 100×90×1.65	10	230	335	HS 90×40×1.65
WALJ	Weak	DCNP 95×80×10×1.9	100×100×2	250	HS 100×90×1.65	10	230	335	HS 90×40×1.65

The pocket consists of a whole pocket and a split pocket. The whole pocket, with a depth of 250 mm, utilizes an HS profile measuring 100 × 90 × 1.65 mm in the beam joint section. It features a notch measuring 230 mm in length and 10 mm in width to facilitate the installation of the beam section. On the other hand, the split pocket, with a depth of 335 mm, uses an HS profile measuring 100 × 45 × 1.65 mm for the strong axis of the joint and an HS profile measuring 100 × 40 × 1.65 mm for the weak axis of the joint. A stiffener is utilized via a triangular thin plate with dimensions of 100 × 100 × 2 mm to connect the whole pocket and the split pocket between the column and beam joints. The study is meant to strengthen the split pocket on the column with the whole pocket on the beam.

Additionally, the split pocket has a clamp at the edge of the notch of the whole pocket to lock the pocket with the column or beam. The bottom of the pocket has six clamps, while the split pocket has four clamps on the upper and lower surfaces. These clamps employ bolts with a diameter of 10 mm and a bolt quality 8.8. Finally, axial loading tests are repeated for each specimen with the following bolt pretensions: 2.5, 5, 7.5, and 10 kN.

3.3. Material Properties

The material properties were determined by testing tensile, referencing SNI 8389:2017, the Indonesian standard on the method of metal testing [26]. The tests were conducted on two samples for the DCNP and two samples for the HS profile. The average values of the yield strength (f_y) and ultimate tensile strength (f_u) are shown in Table 3.

Table 3. Material properties of the CSPM specimens

Steel types	Thickness (mm)	f_y (MPa)	f_u (MPa)
DCNP-1	1.90	275.07	352.33
DCNP-2	1.90	270.76	346.80
Average DCNP	1.90	272.92	349.56
HS-1	1.65	287.96	374.67
HS-2	1.65	281.60	358.57
Average HS	1.65	284.78	366.62

3.4. Test Set-Up

The study tested the CSPM beam-column joints for frictional tensile resistance in instant homes made of prefabricated steel with double-channel cross-sections. The test set-up included a specimen set-up, a horizontal actuator with a 250 kN capacity, a load cell with a capacity of 20 kN, a linear variable differential transformer (LVDT) that was 300 mm long, pin support, and a concrete block. The experimental loading schematics of the specimens are shown in Figure 7. The specimens were installed with an LVDT to measure the displacement occurring in the specimens. The experiment was conducted until the target displacement of 250 mm was achieved. Two techniques, namely the torque moment method and tensile force, are available for applying pretension to bolts [20]. In this research, pretension was used with the torque moment method using a torque wrench.

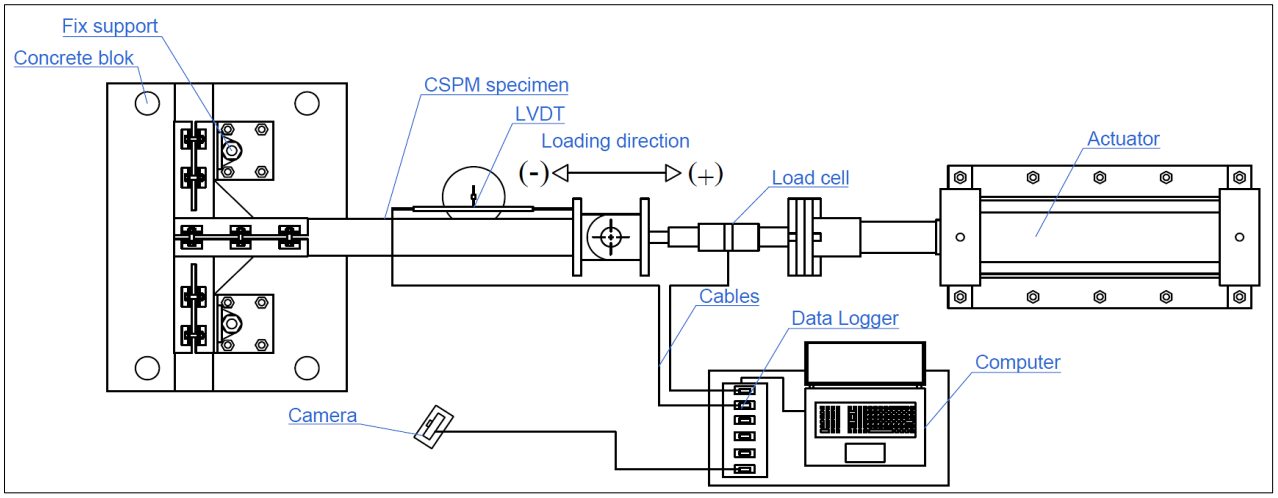

Figure 7. Experimental testing configuration of CSPM as a beam-column joint system

The bolt pre-tensioning of the bolts was implemented in steps. The bolt pretension values given for beam-column joints were 2.50, 5.00, 7.50, and 10.00 kN. The initial pretension was given approximately 2/3 of the targeted pretension on each bolt, and then the new bolt pretension was performed according to the target needed. Pretensioning the bolt in steps was performed to avoid the pretension that changed when the bolts were tightened. This process is called "elastic interaction" [27]. The study was done to ensure that the test object received the same pretension between one bolt and the other bolt, to make the joints between the bolts symmetrical, or to eliminate the gap between the bolt and the plate or the gap between the plate and the plates. The computer then recorded the load and displacement data gathered by the data logger during displacement.

3.5. Pretension Bolts

"Bolt pretension" refers to the initial application of force to the bolt before the application of external force. Bolt pretension can depend on several factors, including bolt condition, bolt size, lubrication of the bolt, and the use of washers. Bolt pretension can be controlled via a torque moment using various equipment, such as a torque wrench, to measure the load stress. The bolt torque refers to the rotational force applied to the pocket and is measured in units of force times length (Nm) [10]. In applying the initial load to the bolt, the bolt torque can be computed by using the relationship between bolt torque and bolt pretension, as shown in Equation 1 [24].

$$T = F \times k \times d \tag{1}$$

where T is the bolt torque, F is the bolt pretension, k is the bolt diameter, and k is the bolt nut factor. For steel fastening in general, the nut factor has a value of 0.3, as shown in Table 4. Bolt pretension plays a critical role in determining the torque of the bolt used. Bolt pretension, however, results in tension on the screw section of the bolt, and over-pretensioning can cause damage to the washer area, bolt thread failure, or bolt head area [24].

Table 4. Nut factor coefficients [28]

Bolt condition	Nut factor (k)
Non-plated, black finish	0.30
Zinc-plated	0.20
Lubricated	0.18
Cadmium-plated	0.16
With Bowman Anti-Seize	0.12
With Bowman-Grip nut	0.09

3.6. Slip Coefficients

The slip coefficient, μ, for one test specimen can be computed using Equation 2 [25]. The slip coefficient, also known as the "friction coefficient," refers to the ratio of the slip load to the clamping force. The value of the coefficient of friction, which is inversely proportional to the pretension of the bolt, can be obtained at the point of peak slip resistance or the point of peak F-d.

$$Slip\ coefficient, \mu = \frac{Slip\ load}{Clamping\ force \times number\ of\ slip\ planes} \tag{2}$$

4. Results and Discussion

4.1. Frictional Tensile Resistance of the Slip-Resistant Bolted Joints

4.1.1. Force-Displacement Behavior

We observed the F-d behavior during the frictional tensile resistance of slip-resistant bolted joints. The results of the frictional tensile resistance of slip-resistant bolted joints testing indicate that the F-d behavior is linear until it reaches the peak point and then relatively decreases and stabilizes at a certain value. The peak point of the F-d curve is defined as the slip resistance, also referred to as the "sticky slip force" [21]. The F-d after reaching the slip resistance point is defined as the "post-slip force." The F-d curve frictional tensile resistance of the slip-resistant bolted joints is shown in Figure 8. This F-d curve is observed at various pretensions to obtain the respective slip resistances. The peak points of the frictional tensile resistance curve for HCHTC specimens range from 4.94 to 13.23 kN, with a displacement range of 0.93 to 2.00 mm. The peak points of the frictional tensile resistance for HCHC- 1 specimens range from 4.98 to 6.94 kN, with a displacement range of 0.70 to 1.80 mm. The peak points of the frictional tensile resistance for HCHC-2 specimens range from 4.49 to 8.38 kN, with a displacement range of 0.65 to 1.89 mm. Meanwhile, the HCHTC specimen exhibits the highest peak frictional resistance point with a pretension of 7.00 kN, which is equivalent to a bolt torque value of 21 Nm or 13.23 kN. In comparison, the HCHC-2 specimen with a pretension of 1.75 kN, which is equivalent to a bolt torque value of 5.25 Nm or 4.49 kN, displays the lowest peak frictional resistance point.

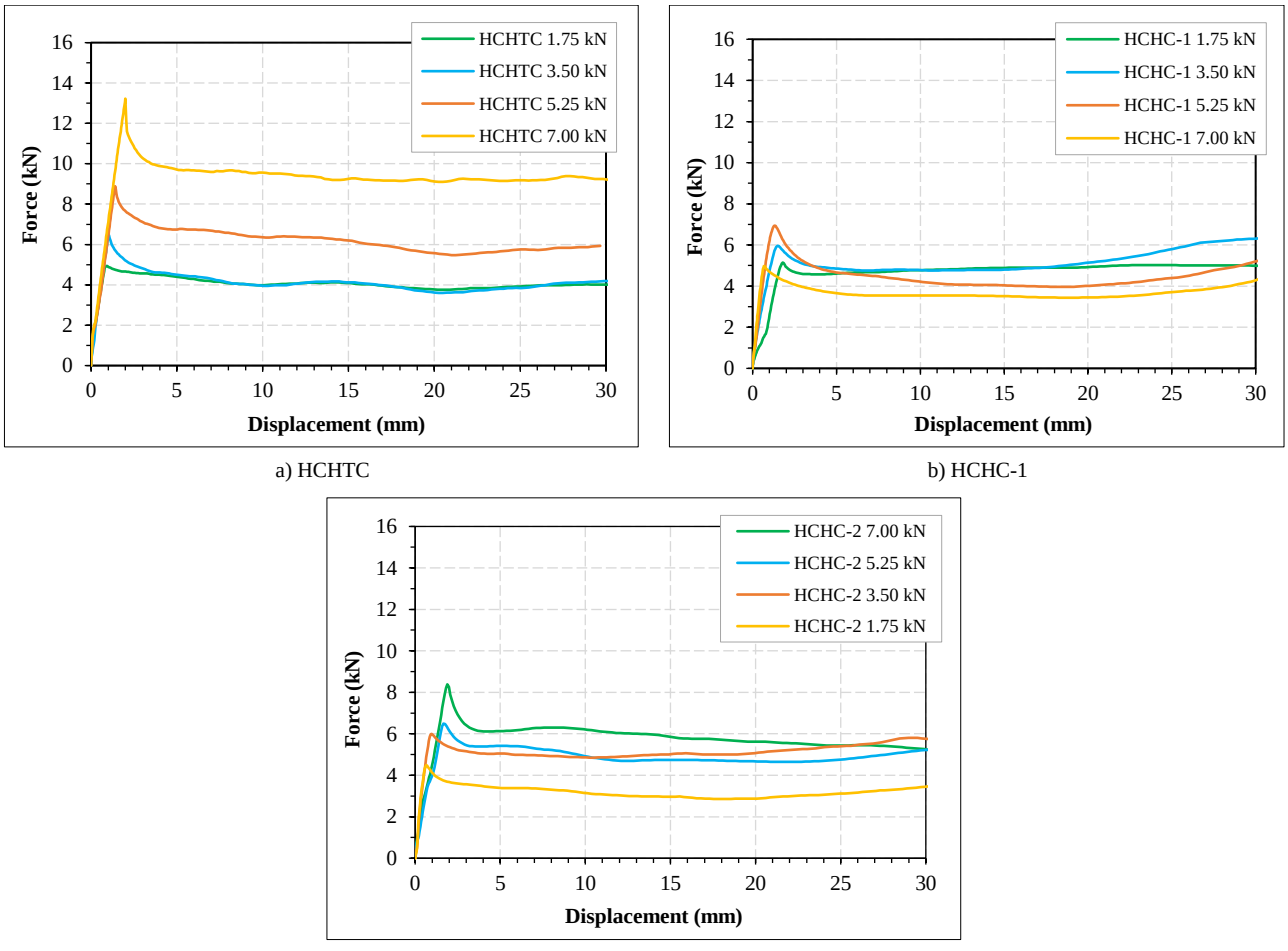

a) HCHTC

b) HCHC-1

c) HCHC-2

Figure 8. Force-displacement: a) HCHTC, b) HCHC-1, and c) HCHC-2

As shown in Figure 8, applying pretensions from small to large and large to small pretensions on the F-d that occurs produces different effects. In particular, the effect of applying a small pretension to large specimens of HCHC results in a greater force than applying a large pretension to a small specimen. The study could be attributed to the fact that applying a large or small pretension may cause the test specimen to experience damage or wear on the plate surface first. In addition to the effects of the sequence of pretension on the bolts, the effect of applying paint to the plate is also observed. Specifically, the F-d curve indicates that the application of paint causes a decrease in F-d. This could be attributed to the fact that the painted plate may have greater roughness than the unpainted plate. The F-d curve data are then processed to calculate the frictional tensile resistance, as shown in Table 5.

Table 5. Results of the frictional tensile resistance testing of the slip-resistant bolted joints

Specimen	Pretension (kN)	Torsi bolt (Nm)	Sticky slip force (kN)	Post slip force (kN)	Displacement (mm)	Average force/bolt (kN)	Average friction/bolt
HCHTC	1.75	5.25	4.94	4.01	0.93	1.23	0.71
	3.50	10.50	6.47	4.00	1.02	1.62	0.46
	5.25	15.75	8.89	6.14	1.40	2.22	0.42
	7.00	21.00	13.23	9.37	2.00	3.31	0.47
HCHC-1	1.75	5.25	5.15	4.84	1.80	1.29	0.74
	3.50	10.50	5.88	4.97	1.65	1.47	0.42
	5.25	15.75	6.94	4.20	1.33	1.73	0.33
	7.00	21.00	4.98	3.53	0.701	1.24	0.18
HCHC-2	7.00	21.00	8.38	5.88	1.89	2.10	0.30
	5.25	15.75	6.49	4.85	1.67	1.62	0.31
	3.50	10.50	6.00	5.03	0.97	1.50	0.43
	1.75	5.25	4.49	3.07	0.65	1.12	0.64

Table 5 shows that the friction coefficient observed is not uniform. In particular, the increase in bolt pretension for HCHTC and HCHC-1 test specimens results in a decrease in the friction coefficient on the surface of the two steel plates. Meanwhile, testing the HCHC-2 specimen by reducing the bolt pretension increases the friction coefficient. This finding is consistent with the research conducted by Heistermann et al. [20] who found that an increase in pretension in bolts leads to a decrease in the friction coefficient on the surface of two steel plates. This research aligns with the findings of Collini et al., who concluded that an increase in bolt-tightening torque reduces the slip factor [23].

Such a decrease is caused by a higher contact area on the pretension, resulting in higher local pressure and a smaller contact area. Meanwhile, for Wang et al., this phenomenon is caused by damage to the surface of the steel that comes into contact, resulting in a decrease in the roughness level of the steel surface [21]. The coefficients of friction for the HCHTC specimen range from 0.47 to 0.71. In particular, the values range from 0.18 to 0.74 and from 0.30 to 0.64 for the HCHC-1 and HCHC-2 specimens, respectively.

The average friction coefficients for the HCHTC, HCHC-1, and HCHC-2 specimens are 0.52, 0.42, and 0.42, respectively. The average friction coefficient values with increasing pretensions for HCHC-1 and HCHC-2 specimens are both equal to 0.42. The average friction coefficient for HCHTC specimens without paint is greater than the average friction coefficient for HCHC specimens with paint. Therefore, the application of paint to different surfaces and pretensions has an impact on the resulting friction coefficients.

Compared to previous studies, the friction coefficient values for slip-resistant bolted joints in this research are coincident, ranging from 0.3 to 0.5. For example, Cruz et al. reported that the friction coefficient for slip-resistant bolted joints on blasted steel surfaces without additional treatment is 0.5, for surfaces blasted and sprayed with zinc or galvanized coating is 0.40, for blasted steel surfaces with a zinc ethyl-silicate coating is 0.40, for surfaces with a zinc epoxy coating is 0.30, and for exposed steel surfaces is 0.50 [18]. Lacey et al. reported that the average friction coefficient for slip-resistant bolted joints using AS/NZS 3678-350 (G350) steel is 0.27 for sandblasted surfaces with clean mill scale (Sa 0) and 0.50 for (Sa 3) [19]. Heistermann et al. concluded that slip-resistant bolted joints using S275 and S690 grade steel have friction coefficients of 0.47 and 0.50, respectively, with an average friction coefficient of 0.36 for different surface treatments on these steels [20]. Wang et al. recommended friction coefficients of 0.45 for slip-resistant bolted joints between high-strength steel (Q550/Q690 HSS) and low-strength steel (Q235), 0.40 for high-strength steel (Q550/Q690 HSS) and medium-strength steel (Q345), and 0.40 for high-strength steel (Q690 HSS) with low and medium-strength steels (Q235/Q345) [21]. The study conducted by Annan & Chiza on slip-resistant bolted joints found average friction coefficients of 0.36 for SP 6 grade steel and 0.53 for SP 5 grade steel on blast-treated surfaces of Category 3 CAN/CSA G40.21 350AT steel [25].

4.1.2. Effect of Surface Condition on the Frictional Tensile Resistance of Slip-Resistant Bolted Joints

Once the friction tensile resistance of the slip-resistant bolted joints test was completed, the effects of surface conditions were observed by disassembling the specimens and taking photographs of them. The tensile resistance of the slip-resistant bolted joints and the friction between two steel surfaces sliding against each other are shown in Figure 9. This study examines how bolt pretension changes the surface condition of slip-resistant bolted joints. As shown in Figure 9, the influence of surface conditions resulting from the frictional tensile resistance of the slip-resistant bolted joints reveals an uneven damage pattern that is concentrated around the bolt hole. The pretension applied after the frictional tensile resistance testing caused scratching on the surface of the HCHTC specimen. At the same time, the surfaces of the HCHC-1 and HCHC-2 specimens experienced paint peeling along the length of the bolt hole.

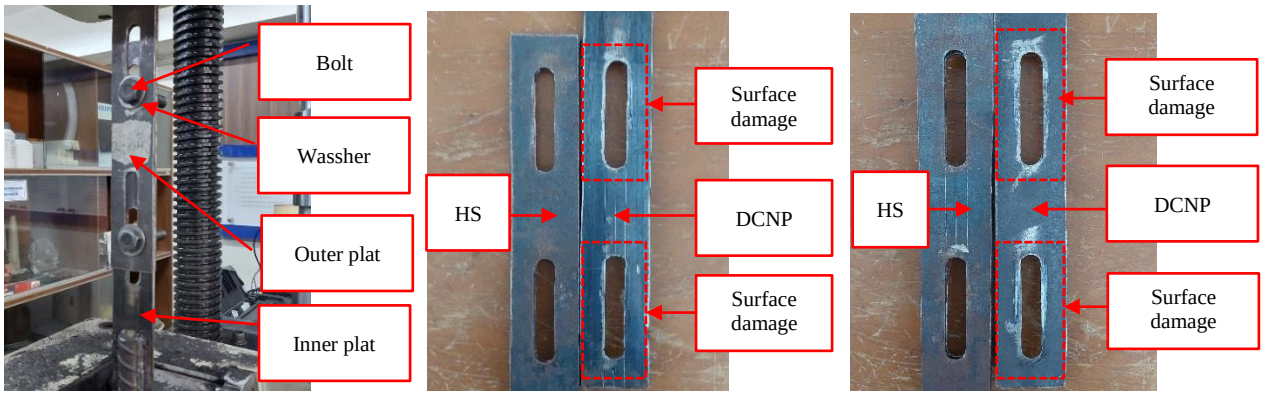

Condition after testing | Front surface view | Back surface view

a) HCHTC

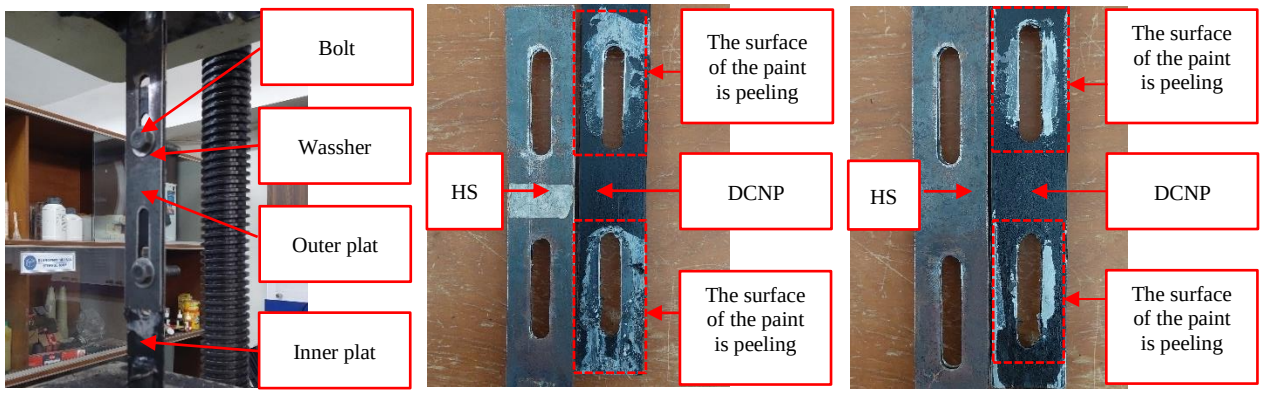

Condition after testing | Front surface view | Back surface view

b) HCHC-1

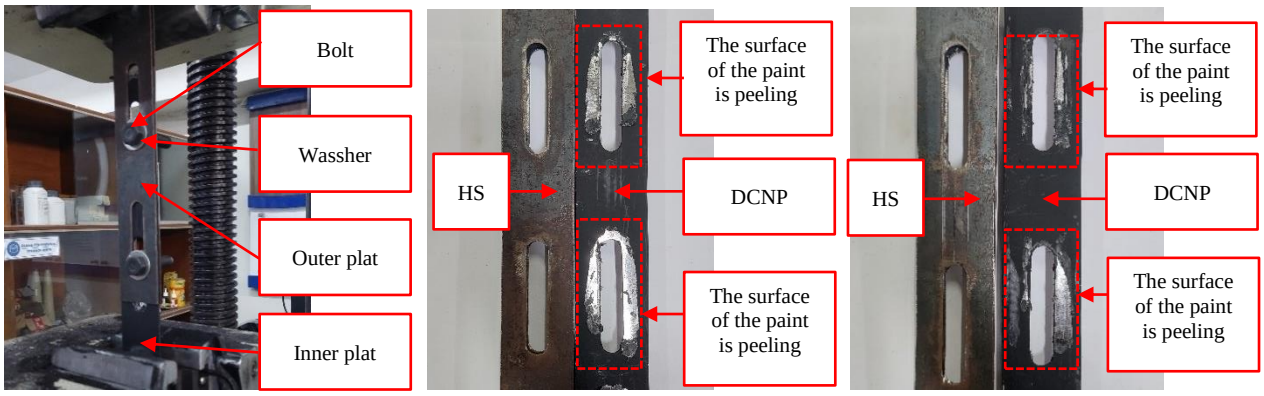

Condition after testing | Front surface view | Back

c) HCHC-2

Figure 9. Conditions after the frictional tensile resistance testing of slip-resistant bolted joints

4.2. Frictional Tensile Resistance of the CSPM Bolted Joint System

4.2.1. Force-Displacement Behavior

One way to compare the frictional tensile resistance of a beam-column joint system made of CSPM is to test it for frictional tensile resistance. The F-d behaviors of 4 specimens under four different pretensions of 2.50, 5.00, 7.50, and 10.00 kN were plotted on a single curve, resulting in 4 distinct curves, respectively, as shown in Figure 10.

The peak points of the frictional tensile resistance in beam-column joints for the SATJ specimen range from 7.72 to 17.73 kN, with a displacement range of 8.28–11.25 mm. The peak tensile resistance points in beam-column joints for the WATJ specimen range from 9.91 to 14.79 kN, with a displacement range of 3.22 to 10.02 mm. The peak points of the frictional tensile resistance in beam-column joints for the SALJ specimen range from 12.54 to 17.57 kN, with a displacement range of 11.19–28.57 mm, while the peak points of the frictional tensile resistance in beam-column joints for the WALJ specimen range from 8.92 to 14.87 kN, with a displacement range of 6.87 to 17.09 mm. The highest peak

frictional resistance point is exhibited by the SATJ specimen with a pretension of 10.00 kN, which is equivalent to a bolt torque value of 30.00 Nm or 17.73 kN. The SATJ specimen shows the lowest peak frictional resistance point with a pretension of 2.50 kN, which is equivalent to a bolt torque value of 7.50 Nm or 7.72 kN.

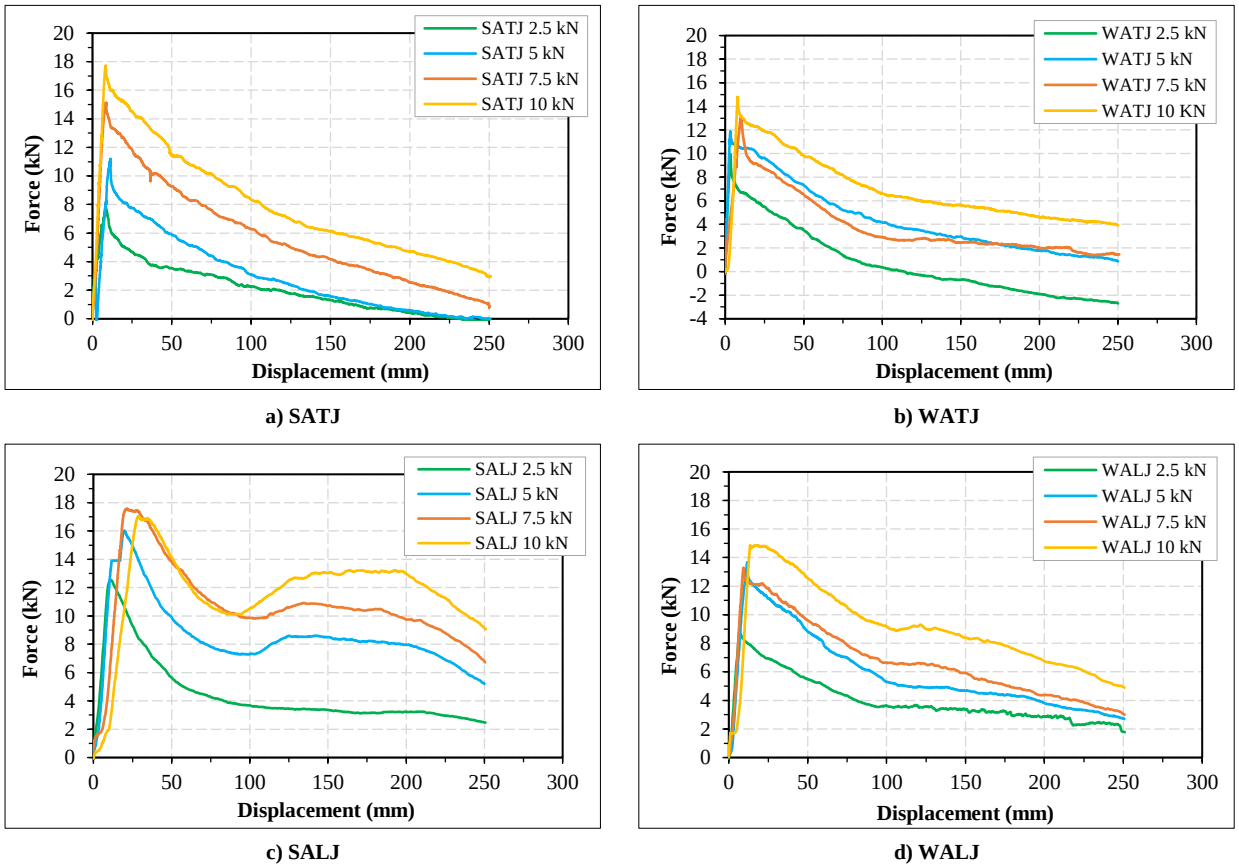

Figure 10. Force–displacement frictional tensile resistance of CSPM beam-column joint systems

The F-d that occurs for both the T joint and L joint is larger along the strong axis than the F-d along the weak axis of the T joint and L joint joints. These results could be attributed to the larger contact area of the pocket along the strong axis compared with the weak axis. The contact area of the clamp on one side, which is clamped to the strong axis joint, has dimensions of 45×2 mm, while the weak axis joint has dimensions of 40×2 mm, with a pocket depth of 335 mm, as shown in Figure 6. The contact area of the strong axis clamp is 30.15 mm^2, while the weak axis joint has an area of 26.80 mm^2. The F-d data were processed to calculate the frictional tensile resistance, as shown in Table 6. The increase in contact area between steel surfaces leads to an increase in the slip factor. In this case, the increase in slip factor can be attributed to the critical plastic slip deformation between two contacting steel surfaces prior to slip failure [21].

Table 6. Results of the frictional tensile resistance testing of the CSPM bolted joint system

Specimen	Pretension (kN)	Torsi bolt (Nm)	Sticky slip force (kN)	Post slip force (kN)	Displacement (mm)	Average force/bolt (kN)	Average friction/bolt
SATJ	2.50	7.50	7.72	2.31	8.42	0.64	0.26
	5.00	15.00	11.19	3.59	11.25	0.93	0.19
	7.50	22.50	15.12	6.71	8.61	1.26	0.17
	10.00	30.00	17.73	9.43	8.28	1.48	0.15
WATJ	2.50	7.50	9.91	1.65	3.38	0.83	0.33
	5.00	15.00	11.86	4.81	3.22	0.99	0.20
	7.50	22.50	13.21	3.94	10.02	1.10	0.15
	10.00	30.00	14.79	7.23	7.93	1.23	0.12
SALJ	2.50	7.50	12.54	4.88	11.19	1.04	0.42
	5.00	15.00	16.02	8.68	19.70	1.34	0.27
	7.50	22.50	17.57	12.72	21.42	1.46	0.20
	10.00	30.00	17.01	13.05	28.57	1.42	0.14
WALJ	2.50	7.50	8.92	4.10	6.87	0.74	0.30
	5.00	15.00	13.65	6.76	11.70	1.14	0.23
	7.50	22.50	13.27	8.43	9.22	1.11	0.15
	10.00	30.00	14.87	10.76	17.09	1.24	0.12

Based on Table 6, the increase in bolt pretension for the SATJ, WATJ, SALJ, and WALJ test specimens resulted in a decrease in the friction coefficient on the surface of the CSPM beam-column joint system. This study is in line with the findings of research by Heistermann et al., which show that increasing bolt pretension causes the friction coefficient on the surfaces of the two steel plates to decrease [20]. This research aligns with the findings of Collini et al., who concluded that an increase in bolt-tightening torque reduces the slip factor [23]. The coefficient of friction in the frictional tensile resistance testing of the CSPM beam-column joint system is less compared to the frictional tensile resistance testing of the CSPM bolted joint system. It is possible that this is because the contact area is more evenly spread out in the CSPM bolted joint system frictional tensile resistance test because the sliding slip-resistant bolted joints are more integrated than in the CSPM joint system frictional tensile resistance test.

The average friction coefficients for the SATJ, WATJ, SALJ, and WALJ specimens are, respectively, 0.19, 0.20, 0.26, and 0.20. The SALJ specimen indicates the average value of the maximum coefficient of friction, whereas the SATJ specimen indicates the average value of the minimum coefficient of friction.

4.2.2. Effect of Surface Condition Frictional Tensile Resistance on the CSPM Bolted Joint System

The contact area in the frictional tensile resistance of the beam-column joint system is unevenly distributed between the inner surface of the pocket and the outer surface of the column. In the initial condition, there is no contact between the pocket and the column when the pretension is zero, as shown in Figure 11-a. When the bolt is given pretension that is converted using the torque moment value, the clamp will experience compression, as shown in Figure 11-b. Clamps have a greater thickness than pocket joints, causing the pocket joints to change shape. In turn, this change in shape causes the contact area between the column and the pocket to change from its initial condition. The dominant contact area is located on the upper surface of the middle side and the side surface of the middle side. In this case, the dominant contact area caused by this pretension is referred to as the "effective surface pressure area."

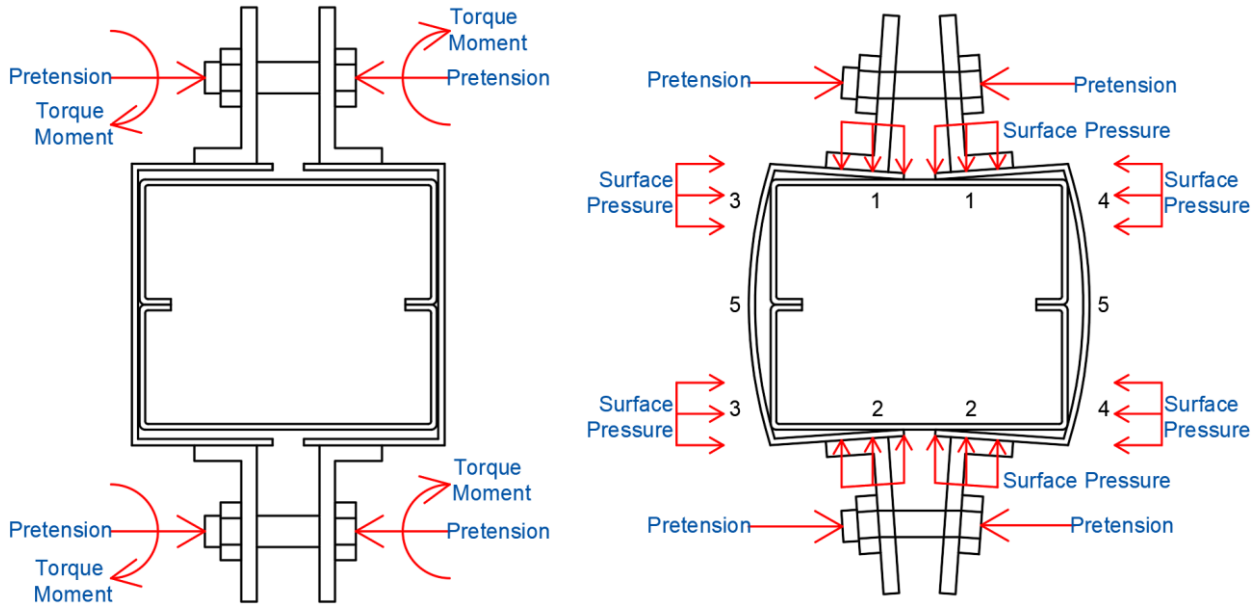

a) Pocket section state before the initial pretension force

b) Pocket section state in the final set of pretension force

Figure 11. The condition of the test specimen is due to pretension forces in the beam-column joint system

The pretension of the CSPM as a beam-column joint system for this prefabricated steel instant house must be limited. Applying too little pretension is considered suboptimal as it can result in a significant gap between the outer surface of the column and the inner surface of the split pocket. This significant gap will cause the beam-column joint system to split when subjected to lateral forces. In addition, excessive pretension can lead to column damage due to clamping force effects, cause the bolt to have shear failure, and cause the clamp to experience high compressive conditions. The pressure condition on the clamp, as shown in Figure 11b, will result in Zones 1–4 experiencing compression and Zone 5 experiencing tension, causing the surface around Zone 5 to bend. The pressure condition on this clamp causes effective surface pressure to occur only in Zones 1–4.

As shown in Figure 12, the uneven friction contact area can be seen on the member surface, where the paint is peeling off after testing. The contact area of friction on the upper and lower surfaces between the split pocket and the longitudinal column mostly occurs in the center of the column. The dominant friction contact area is at the edge of the column on the side area of the split pocket surface and column. The surface of the split pocket with a column joint system on the top and bottom sides has peeling paint, a condition that affects the middle surface, which serves as proof of this phenomenon. On the side surfaces, the paint peeling occurs more on the edge of the column.

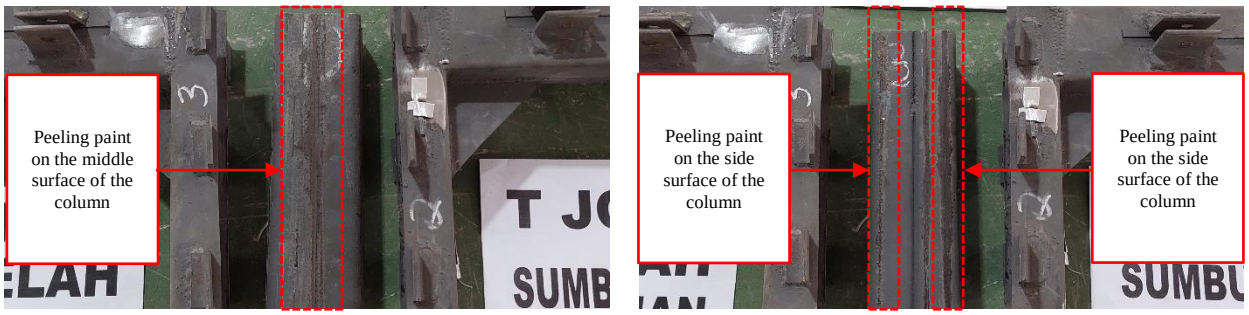

Front surface view of the SATJ test specimen Side surface view of the SATJ test specimen

a) SATJ

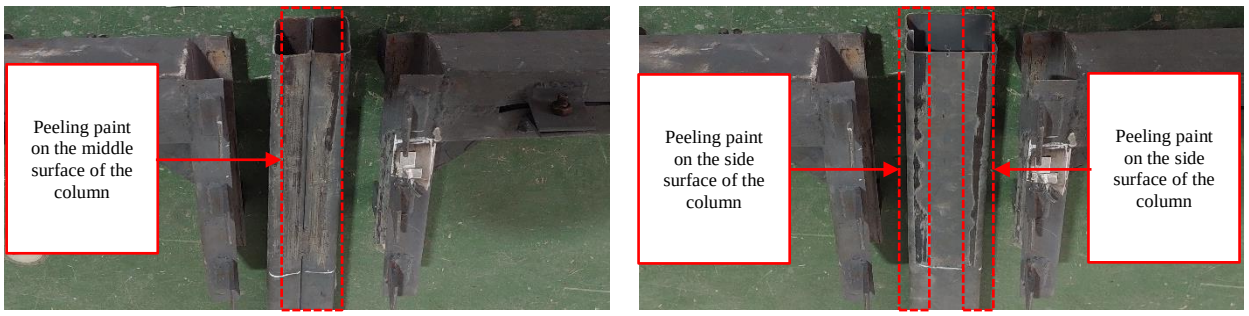

Front surface view of the WATJ test specimen Side surface view of the WATJ test specimen

b) WATJ

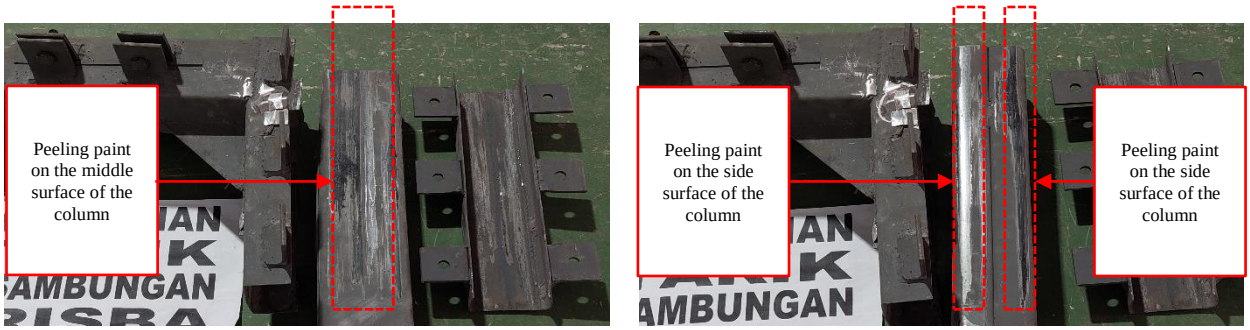

Front surface view of the SALJ test specimen Side surface view of the SALJ test specimen

c) SALJ

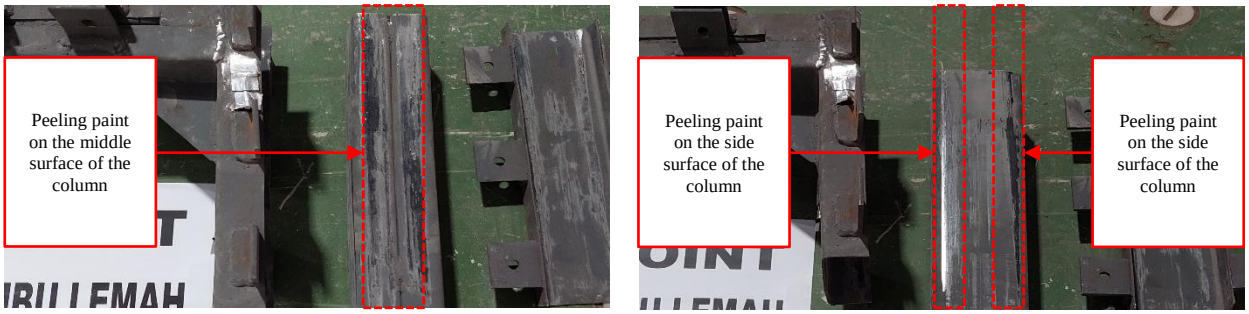

Front surface view of the WALJ test specimen Side surface view of the WALJ test specimen

d) WALJ

Figure 12. Conditions after testing the frictional tensile resistance of the beam-column joint system

Overall, the study on the frictional resistance of the CSPM beam-column joint system in instant homes made of prefabricated steel can be used as a guide for designing the clamping force in bolted joint systems. Referring to the study by Sutrisno et al. [7], the maximum lateral strength of instant steel houses with nine columns was found to be 18 kN, with each steel column capable of carrying 2 kN of lateral force. Based on the lateral force value, the joint system must be able to support a force of 2 kN. Therefore, as shown in Figure 13, the joint system between the ring beam and column with two pairs of clamping clamps, with a friction coefficient of 0.2, requires a minimum pretension force of 2.5 kN.

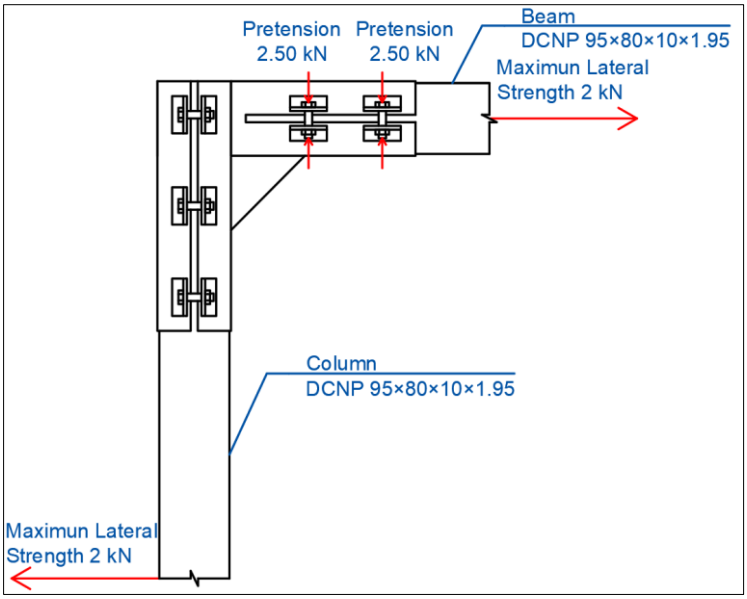

Figure 13. Clamping force in bolted joints

5. Conclusions

Based on the experimental testing of the frictional tensile resistance of CSPM as a beam-column joint system, the following conclusions can be drawn:

- The effective friction coefficient of beam-column joint system specimens is in the range of 0.19–0.26. Thus, the friction coefficient is lower than that of slip-resistant bolted joint specimens, which ranges from 0.42 to 0.52. Several factors, including the bolt pretension used, the contact area of the steel surfaces, and the effects of surface treatment on the steel, influence the friction coefficient.
- The friction coefficient has an inversely proportional relationship with bolt pretension; thus, an increase in bolt pretension causes a decrease in the friction coefficient at the surface contact of the beam-column CSPM. The decrease in friction coefficient is caused by the deterioration of surface contact roughness on the outer surface of the element member, which interacts with the contact surface of the pocket at a certain pressure.
- The clamp's pressure from the bolt pretension induces the surface contact deformation of the pocket surface, thus creating a bumpy surface contact area between the inner surface of the pocket and the outer surface of the element members. As such, the effective surface friction resistance area is the surface contact between the outer surface of the element members and the inner surface of the pocket.
- In accordance with the verification done with the predecessor study, the proposed CSPM joint system could achieve sufficient capacity to resist lateral force demand from the full-scaled test of an instant house structure made of steel in terms of its maximum lateral strength.

6. Declarations

6.1. Author Contributions

Conceptualization, W.T.P., A.F.S., A.S., I.S., and H.Y.P.; methodology, W.T.P., A.F.S., A.S., I.S., and H.Y.P.; validation, W.T.P.; formal analysis, W.T.P., A.F.S., and A.S.; writing—original draft preparation, W.T.P., A.F.S., A.S., I.S., and H.Y.P.; writing—review and editing, W.T.P., A.F.S., A.S., I.S., and H.Y.P.; supervision, A.F.S., A.S., and I.S. All authors have read and agreed to the published version of the manuscript.

6.2. Data Availability Statement

The data presented in this study are available in the article.

6.3. Funding and Acknowledgments

The authors would like to express their gratitude to the Research Directorate of Universitas Gadjah Mada for the support (Grant No. 5075/UN1.P.II/Dit-Lit/PT.01.01/2023). The authors are also grateful to the Structural Laboratory and Construction Material Laboratory under the Department of Civil and Environmental Engineering, Faculty of Engineering, Universitas Gadjah Mada, for the experimental testing facilitation. We are also grateful to the Badan Penerbit dan Publikasi Universitas Gadjah Mada for their assistance in proofreading this manuscript. The CSPM joint system was also registered in a patent with the number P00202200431.

6.4. Conflicts of Interest

The authors declare no conflict of interest.

7. References

[1] Librian, V., Ramdhan, M., Nugraha, A. D., Mukti, M. M., Syuhada, S., Lühr, B. G., Widiyantoro, S., Mursitantyo, A., Anggraini, A., Zulfakriza, Z., Muttaqy, F., & Mi'rojul Husni, Y. (2024). Detailed seismic structure beneath the earthquake zone of Yogyakarta 2006 (Mw ~6.4), Indonesia, from local earthquake tomography. Physics of the Earth and Planetary Interiors, 351, 107170. doi:10.1016/j.pepi.2024.107170.

[2] Mason, H. B., Montgomery, J., Gallant, A. P., Hutabarat, D., Reed, A. N., Wartman, J., Irsyam, M., Simatupang, P. T., Alatas, I. M., Prakoso, W. A., Djarwadi, D., Hanifa, R., Rahardjo, P., Faizal, L., Harnanto, D. S., Kawanda, A., Himawan, A., & Yasin, W. (2021). East Palu Valley flowslides induced by the 2018 MW 7.5 Palu-Donggala earthquake. Geomorphology, 373. doi:10.1016/j.geomorph.2020.107482.

[3] Yulianto, E., Yusanta, D. A., Utari, P., & Satyawan, I. A. (2021). Community adaptation and action during the emergency response phase: Case study of natural disasters in Palu, Indonesia. International Journal of Disaster Risk Reduction, 65(September), 102557. doi:10.1016/j.ijdrr.2021.102557.

[4] Central Sulawesi Provincial Government. (2019). Finalization Report of Data and Information on Earthquake, Tsunami and Liquefaction Disasters PADAGIMO in Central Sulawesi as of January 30, 2019. Central Sulawesi Provincial Government, Palu, Indonesia. (In Indonesian).

[5] Setyonugroho, G. A., & Maki, N. (2024). Policy implementation model review of the post-disaster housing reconstruction in Indonesia case study: Aceh, Yogyakarta, and Lombok. International Journal of Disaster Risk Reduction, 100, 1–18. doi:10.1016/j.ijdrr.2023.104181.

[6] Pribadi, K. S., Abduh, M., Wirahadikusumah, R. D., Hanifa, N. R., Irsyam, M., Kusumaningrum, P., & Puri, E. (2021). Learning from past earthquake disasters: The need for knowledge management system to enhance infrastructure resilience in Indonesia. International Journal of Disaster Risk Reduction, 64, 102424. doi:10.1016/j.ijdrr.2021.102424.

[7] Sutrisno, W., Satyarno, I., Awaludin, A., Saputra, A., & Setiawan, A.F. (2022). Seismic Performance of Instant Steel Frame House for Post Earthquake Reconstruction. Proceedings of the 5th International Conference on Sustainable Civil Engineering Structures and Construction Materials. SCESCM 2020, Lecture Notes in Civil Engineering, 215, Springer, Singapore. doi:10.1007/978-981-16-7924-7_6.

[8] Zhang, Z., Li, D., Wang, H., Li, S., Qian, H., Bi, Y., Wang, G., Jin, X., & Fan, F. (2024). Static and Seismic Experimental Study of Novel Prefabricated Beam-Column Joints with Elongated-Hole Brackets. International Journal of Steel Structures, 24(1), 118–131. doi:10.1007/s13296-023-00804-5.

[9] Wang, H., Zhang, B., Qian, H., Liu, J., An, B., & Fan, F. (2021). Experimental and numerical studies of a new prefabricated steel frame joint without field-welding: Design and static performance. Thin-Walled Structures, 159, 107271. doi:10.1016/j.tws.2020.107271.

[10] Lokesh Kumar, P. J., Vasanthe Roy, J., & Sevvel, P. (2023). An investigation on the influence of torque and R-ratio on the fatigue life of double-lap bolted joint using FEM. Materials Today: Proceedings. doi:10.1016/j.matpr.2023.05.342.

[11] Mahmoudi, M., Kosari, M., Lorestani, M., & Jalili Sadr Abad, M. (2020). Effect of contact surface type on the slip resistance in bolted connections. Journal of Constructional Steel Research, 166, 1–12. doi:10.1016/j.jcsr.2020.105943.

[12] Deng, E. F., Zong, L., Ding, Y., Zhang, Z., Zhang, J. F., Shi, F. W., Cai, L. M., & Gao, S. C. (2020). Seismic performance of mid-to-high rise modular steel construction - A critical review. Thin-Walled Structures, 155, 106924. doi:10.1016/j.tws.2020.106924.

[13] Qin, J., & Tan, P. (2022). Design method of innovative box connections for modular steel constructions. Journal of Building Engineering, 57, 104820. doi:10.1016/j.jobe.2022.104820.

[14] Bazarchi, E., Davaran, A., Lamarche, C. P., Roy, N., & Parent, S. (2023). Experimental and numerical investigation of a novel vertically unconstrained steel inter-modular connection. Thin-Walled Structures, 183, 110364. doi:10.1016/j.tws.2022.110364.

[15] Fajar, A.S., Saputra, A., Satyarno, I., & Himawan, L. (2022). Investigation of Fast Connection (Clamped Pocket Mechanics) for Modular Instant Steel House with Finite Element Analysis: Back to Build Post-disaster. Proceedings of the 5th International Conference on Sustainable Civil Engineering Structures and Construction Materials, SCESCM 2020, Lecture Notes in Civil Engineering, 215, Springer, Singapore. doi:10.1007/978-981-16-7924-7_50.

[16] Gunawardena, T. (2016). Behaviour of prefabricated modular buildings subjected to lateral loads. Ph.D. Thesis, The University of Melbourne, Melbourne, Australia.

[17] Maiorana, E., Zampieri, P., & Pellegrino, C. (2018). Experimental tests on slip factor in friction joints: Comparison between european and American standards. Frattura Ed Integrita Strutturale, 12(43), 205–217. doi:10.3221/IGF-ESIS.43.16.

[18] Cruz, A., Simões, R., & Alves, R. (2012). Slip factor in slip resistant joints with high strength steel. Journal of Constructional Steel Research, 70, 280–288. doi:10.1016/j.jcsr.2011.11.001.

[19] Lacey, A. W., Chen, W., Hao, H., & Bi, K. (2019). Experimental and numerical study of the slip factor for G350-steel bolted connections. Journal of Constructional Steel Research, 158, 576–590. doi:10.1016/j.jcsr.2019.04.012.

[20] Heistermann, C., Veljkovic, M., Simões, R., Rebelo, C., & Simões da Silva, L. (2013). Design of slip resistant lap joints with long open slotted holes. Journal of Constructional Steel Research, 82, 223–233. doi:10.1016/j.jcsr.2012.11.012.

[21] Wang, Y. B., Wang, Y. Z., Chen, K., & Li, G. Q. (2020). Slip factor between shot blasted mild steel and high strength steel surfaces. Journal of Constructional Steel Research, 168, 105969. doi:10.1016/j.jcsr.2020.105969.

[22] Lacey, A. W., Chen, W., Hao, H., & Bi, K. (2018). Structural response of modular buildings – An overview. Journal of Building Engineering, 16, 45–56. doi:10.1016/j.jobe.2017.12.008.

[23] Collini, L., Garziera, R., Corvi, A., & Cantarelli, G. (2024). Slip strength of COR-TEN and Zn-coated steel preloaded bolted joints. Results in Engineering, 22, 102009. doi:10.1016/j.rineng.2024.102009.

[24] Patne, S., Karale, A., Mohankumar, V., & Rane, S. (2023). Bolt pre-load CAE analysis and validation: FEA simulation of hex bolt tightening torque for IDU assembly of 2-wheeler in MSC Nastran and practical validation. Materials Today: Proceedings, 72, 1925–1928. doi:10.1016/j.matpr.2022.10.155.

[25] Annan, C. D., & Chiza, A. (2013). Characterization of slip resistance of high strength bolted connections with zinc-based metallized faying surfaces. Engineering Structures, 56, 2187–2196. doi:10.1016/j.engstruct.2013.08.040.

[26] SNI 8389:2017. (2017). Metal Tensile Test Method. Badan Standardisasi Nasional, Jakarta, Indonesia. (in Indonesian).

[27] Link, R. (1991). An Introduction to the Design and Behavior of Bolted Joints. Journal of Testing and Evaluation, 19(5), 417–418. doi:10.1520/jte12600j.

[28] Budynas, R. G., & Nisbett, J. K. (2011). Shigley's mechanical engineering design. McGraw-Hill, New York, United States.